Water Science and Engineering xxxx, xxx(xxx): xxx

HOSTED BY

ELSEVIER

Available online at www.sciencedirect.com

Water Science and Engineering

journal homepage: wse.hhu.edu.cn

Hydraulic characteristics and flow trajectories under two-sided asymmetric inflow conditions for a deep storage tunnel system

Wei He [a,b,c,d], Chao Yu [a,b,c], Xiao-dong Yu [a,b,c,*], Jian Zhang [a,b,c], Jose G. Vasconcelos [e], Hui Xu [a,b,c], Shou-ling Chen [f]

[a] College of Water Conservancy and Hydropower Engineering, Hohai University, Nanjing 210098, China
[b] State Key Laboratory of Hydrology–Water Resources and Hydraulic Engineering, Hohai University, Nanjing 210098, China
[c] Collaborative Innovation Center on Water Safety and Water Science, Hohai University, Nanjing 210098, China
[d] Guangdong Yuehai Yuexi Water Supply Company Limited, Zhanjiang 524000, China
[e] Department of Civil and Environmental Engineering, Auburn University, 238 Harbert Engineering Center, Auburn, AL 36849, USA
[f] Jiangsu Province Taihu-Lake Water Resources Planning & Design Institute Company Limited, Suzhou 215000, China

Received 9 November 2022; accepted 15 November 2023
Available online ■ ■ ■

Abstract

Deep storage tunnels (DSTs) are used in densely urbanized areas to relieve stormwater collection systems, thereby reducing urban floods and runoff pollution, due to their substantial storage capacity. The computation of the hydraulic characteristics and flow trajectories of DSTs under rapid filling scenarios can help to predict sediment deposition and pollutant accumulation associated with the stored runoff, as well as the likelihood of operational problems, such as excessive surging. However, such assessments are complicated by various inflow scenarios encountered in tunnel systems during their operation. In this study, the Suzhou River DST in China is selected as a study case. Particles were tracked, and hydraulic analysis was conducted with scaled model experiments and numerical models. The flow field, particle movement, air–water phase, and pressure patterns in the DST were simulated under various one- and two-sided inflow scenarios. The results showed that with regards to the design conditions involving two-sided inflows, flow reversals occurred with stepwise increases in the water surface and pressure. In contrast, this phenomenon was not observed under the one-sided inflow scenario. Under the asymmetric two-sided inflow scenarios, water inflows led to particle accumulation near the shaft, reducing the received inflows. However, under the symmetric inflow conditions, particles were concentrated near the middle of the tunnel. Compared to those under the symmetric inflow scenario, asymmetric inflow caused surface wave and entrapped air reductions. This study could provide support for regulation of the inflow of the Suzhou River DST and for prediction of sediment and pollutant accumulation.

Keywords: Deep storage tunnel; Flow trajectory; Hydraulic characteristic; Hydrodynamic and particle simulation; Physical model test

1. Introduction

Deep storage tunnels (DSTs) are large-scale storage and conveyance tunnel systems that have been adopted in highly urbanized cities to provide relief for stormwater collection systems, reduce flooding episodes, and decrease runoff pollution. These systems typically include collection system diversion components, inflow shafts, and underground tunnels. Underground tunnels are typically the main component that

This work was supported by the National Natural Science Foundation of Jiangsu Province (Grant No. BK20230099), the National Natural Science Foundation of China (Grants No. 52379061 and 52179062), and the Key Laboratory of Water Grid Project and Regulation of Ministry of Water Resources (Grant No. QTKS0034W23292).

* Corresponding author.
E-mail address: yuxiaodong_851@hhu.edu.cn (Xiao-dong Yu).

Peer review under responsibility of Hohai University.

https://doi.org/10.1016/j.wse.2023.11.006

stores runoff. DST systems have been adopted in cities worldwide, including large cities in China (Wu et al., 2016), and have demonstrated their practicality in mitigating urban flooding and reducing runoff pollution (Higuchi et al., 1994; Catano-Lopera et al., 2014; Vasconcelos and Wright, 2017; Pachaly et al., 2021),.

The transition between free-surface and pressurized flow regimes, referred to as mixed flows, often occurs in sewer and tunnel systems undergoing rapid filling events, and understanding its hydraulic characteristics could help to avoid operational issues (Vasconcelos and Wright, 2017). There has been much research focusing on the modeling of stormwater systems undergoing pressurization. Finite volume models include the Illinois transient model (ITM) (Leon et al., 2011; Catano-Lopera et al., 2014) and the hydraulic analysis of sewers and tunnels (HAST) model (Hatcher et al., 2015; Pachaly et al., 2021), both capable of performing one-dimensional (1-D) system-wide tunnel simulations. Models based on the method of characteristics (MOC) have also been developed to simulate mixed flow conditions by tracking pressurization interfaces (Song et al., 1983; Vasconcelos and Wright, 2003; Duan, 2015; Hatcher et al., 2015). Guo and Zhou (2006) developed the precise integration method to improve the numerical stability in obtaining free-surface and pressurized flow regimes by adding a virtual time term to the Saint−Venant equations.

Three-dimensional (3-D) computational fluid dynamics (CFD) tools have recently been adopted in the hydraulic simulation of tunnel systems undergoing pressurization. Due to the high computational effort, most system-wide simulations are not practical. Instead, these models can describe flows in smaller regions of DSTs or even within a given hydraulic structure of the system. As a supplement to the results of system-wide 1-D models, 3-D simulations can provide more details of the air−water distribution and free-surface shapes with interface tracking methods, such as the volume of fluid (VOF) method (Hirt and Nichols, 1981; Cheng et al., 2010; Zhou et al., 2018). 3-D modeling has also been performed to study the effects of ventilation in shafts and manhole covers under the conditions of inertial oscillations or a sudden release of air pockets (Wang and Vasconcelos, 2018, 2020).

Under real-world inflow conditions, flow transients are observed in hydraulic systems undergoing filling, which induce irregular changes in the velocity, pressure, and air−water distribution within tunnels (Lingireddy et al., 2004; Epstein, 2008; Pachaly et al., 2020). Such unsteady behaviors can influence the motion of sediment particles and pollutant movement in runoff. Sediment and pollutant distribution modeling is useful to prediction of locations where deposition may occur. Similarly, excessive pressure build-up and surging in tunnels can pose operational issues, such as the return of contaminated water to the grade and manhole cover displacement (Zhou et al., 2018; Li et al., 2018). These phenomena can be predicted with hydraulic modeling. Therefore, a 3-D CFD model was used in this study.

Flow trajectories in DSTs are different from those in traditional collection systems. Traditional stormwater collection systems provide a limited storage capacity, and water flow direction reversal seldom occurs. In contrast, DSTs provide a high storage capacity, can become pressurized, and often encompass multiple inflow points, leading to several inflow fronts. Flow interactions in DSTs are thus more complex, and one consequence is the possibility of water velocity reversal, also referred to herein as reversed flow. The determination of flow trajectories in DST systems is useful for tracking sediments and contaminants in tunnels. However, such tracking in DSTs has not yet been sufficiently investigated. This is one of the important knowledge gaps addressed in this study.

Another relevant issue impacting DST operation is linked to the processes associated with air pocket formation, displacement, and release, often creating additional issues. Rapid inflow conditions lead to the emergence of entrapped pockets through various mechanisms, including shear flow instability and multiple pressurization interfaces (Vasconcelos and Wright, 2006; Vasconcelos et al., 2009; Eldayih et al., 2020). Entrapped air can be discharged from the shaft and can cause intense pressure peaks, air−water surges, and geysers (Wright et al., 2011; Hatcher and Vasconcelos, 2017). The difficulty in precisely locating entrapped air pockets, air entrainment through pressurization, and the ability to control inflows in DSTs influence the management of air−water interactions in tunnels (Li et al., 2018; Malekpour and Karney, 2019; Schulz et al., 2020).

This study aimed to investigate the hydraulic characteristics and flow trajectories under two-sided asymmetric inflow conditions. 3-D CFD flow simulations were performed to reveal air−water interactions, particle tracer movement, pressure evolution and surging, and entrapped air for the first stage of a DST in Shanghai, China, with consideration of various inflow conditions.

2. Materials and methods

2.1. Case study

The first stage of the Suzhou River DST in Shanghai, China, located between the upstream Miaopu (MP) shaft and the downstream Yunlingxi (YLX) shaft (Fig. 1), was selected as the object of the case study. The circular plan area of the inflow shafts has a diameter of 30 m and a depth of 60 m. The DST aims to relieve the collection system and reduce the impact of runoff contamination. The reach length between the two shafts is 1.64 km, with a diameter of 10 m and an average slope of 0.10%. The DST is generally operated in the case of large storms and provides multipurpose networks for underground pipelines. There are facilities to retain bedload sediment before the inflow shaft at the surface, while suspended sediment is the main concern. After operation for storm runoff storage, the stored water is pumped out, and the deposited sediment is dredged. Inflows can enter via both the upstream and downstream shafts, and the design peak inflow rates are 42.16 and 73.84 m^3/s for the MP and YLX shafts, respectively. In both shafts, energy-dissipating and anti-scour facilities for

Please cite this article as: He, W et al., Hydraulic characteristics and flow trajectories under two-sided asymmetric inflow conditions for a deep storage tunnel system, Water Science and Engineering, https://doi.org/10.1016/j.wse.2023.11.006

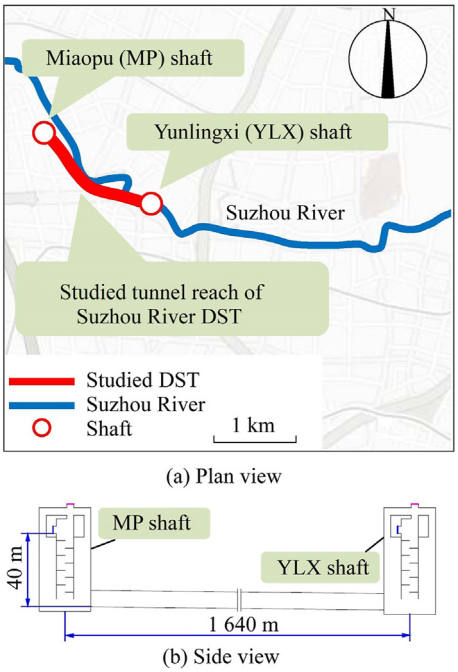

Fig. 1. Plan view and side view of study site.

the inflow water are set, yielding smooth and steady water flow conditions when the inflow water enters the shafts. The operation scheme requires that the inflows into the study reach of the Suzhou DST must be shut down by the sluice gate when the main tunnel is filled and the water pressure of the MP shaft reaches 15 m (approximately 5 m above the tunnel crown) to avoid the occurrence of damaging surges. The combined peak inflows assumed in the design can be normalized with Eq. (1):

$$Q^* = \frac{Q_{\text{peak}}}{\sqrt{gD^5}} \tag{1}$$

where Q^* is the dimensionless discharge, Q_{peak} is the peak discharge of the DST inflow, g is the gravitational acceleration, and D is the section width of the DST. The normalized inflows reached 0.12, lower than the range determined by Vasconcelos and Wright (2017), possibly not causing significant surging issues. Thus, surge evaluation was not included in this study.

2.2. Physical model test

2.2.1. Model setup

As this study focused on a numerical study of the filling process of the Suzhou River DST and related particle tracking, numerical modeling results were validated with the physical model shown in Fig. 2. The physical model considered the Froude similarity principle, with a model-to-prototype scale of 1:30, thus producing a length of 54.67 m and a pipe diameter of 0.33 m. The minimum values of the Reynolds number (Re) and Weber number (We) were around 5.8×10^6 and 4.7×10^4, respectively. Previous studies have shown that laboratory experiments should be conducted in a large facility that operates at relatively high Reynolds numbers (typically Re greater than 2×10^5 to 3×10^5 or $We^{0.5}$ greater than 140) and considers the

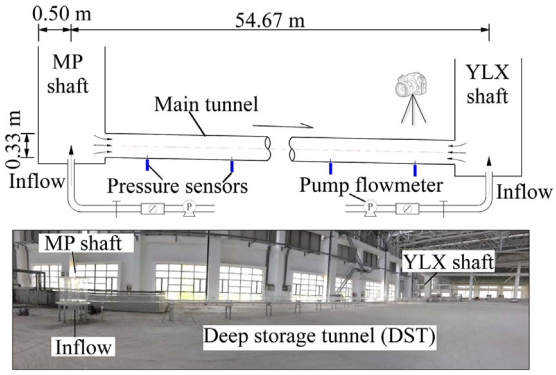

Fig. 2. Schematic arrangement of physical model and test instruments.

scale effects in terms of the void fraction and bubble count rate distribution in small channels with Re less than 4×10^4 (Chanson and Gualtieri, 2008; Pfister and Chanson, 2014; Gualtieri and Chanson, 2021). Therefore, in consideration of entrapped air pockets, the air−water scale effects were insignificant in this study.

The physical model was mainly made of plexiglass covering the two shafts and main tunnel, and the roughness of the smooth concrete in the tunnel was assumed comparable to that of the physical model. In this DST, efficient energy dissipation and deaeration approaches were built into the shafts (Wang et al., 2016; Qi et al., 2019). The shaft inflows entered from the bottom to ensure non-aerated inflows.

2.2.2. Test measurement arrangement

The inflow discharge levels of the two shafts were measured with MIF-S200 electromagnetic flowmeters and flow measurement weirs. The accuracy of the MIF-S200 electromagnetic flowmeter is around 0.2 L/s (around 1%), and the height accuracy of the flow measurement weir is around 0.2 mm. The free surface was recorded and measured with a camera, a water level scale, and a needle water level gauge. The accuracy of the needle water level gauge is around 0.2 mm. Five CY200 pressure sensors were set at the bottoms of the sections 0, 300, 600, 900, and 1 200 m from the upstream MP shaft (prototype) (P1, P2, P3, P4, and P5 in Fig. 3, respectively). The accuracy of the CY200 pressure sensor is around 0.1 m.

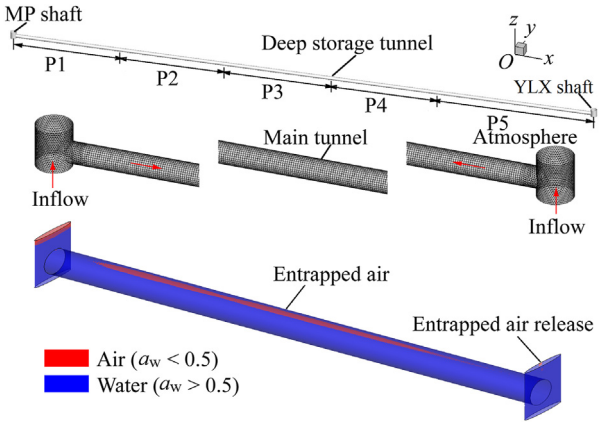

Fig. 3. Mesh grid and air−water phase of numerical model.

Please cite this article as: He, W et al., Hydraulic characteristics and flow trajectories under two-sided asymmetric inflow conditions for a deep storage tunnel system, Water Science and Engineering, https://doi.org/10.1016/j.wse.2023.11.006

2.3. 3-D compressible hydrodynamic and particle numerical model

2.3.1. Governing equations and model solution

A 3-D compressible hydrodynamic and particle numerical model was developed with ANSYS Fluent (ANSYS, 2012; Catano-Lopera et al., 2014; He et al., 2017, 2018; Li et al., 2018; Besharat et al., 2020; Zhao et al., 2022). This model is based on the solution of the Navier−Stokes equations representing the continuity equation (Eq. (2)) and momentum equation (Eq. (3)):

$$\frac{\partial \rho}{\partial t}+\nabla(\rho \boldsymbol{v})=0 \tag{2}$$

$$\frac{\partial}{\partial t}(\rho \boldsymbol{v})+\nabla\cdot(\rho \boldsymbol{v}\boldsymbol{v})=-\nabla \boldsymbol{p}+\nabla\cdot(\overline{\overline{\boldsymbol{\tau}}})+\boldsymbol{F} \tag{3}$$

where ρ is the density, t is the time, $\boldsymbol{v}$ is the velocity component, $\boldsymbol{p}$ is the pressure, $\overline{\overline{\boldsymbol{\tau}}}$ is the stress tensor, and $\boldsymbol{F}$ is the gravitational and external body forces.

The VOF method was used to represent the air−water two-phase flow and identify the free-surface interface. The density was calculated with the following equations (Cheng et al., 2010; Catano-Lopera et al., 2014; Zhou et al., 2018; Qi et al., 2019; Besharat et al., 2020; Wang and Vasconcelos, 2020).

$$\rho=\alpha_{\mathrm{a}}\rho_{\mathrm{a}}+\alpha_{\mathrm{w}}\rho_{\mathrm{w}} \tag{4}$$

$$\alpha_{\mathrm{a}}+\alpha_{\mathrm{w}}=1 \tag{5}$$

where α_{a} and α_{w} are the volume fractions of air and water, respectively; and ρ_{a} and ρ_{w} are the densities of air and water, respectively.

The renormalization group (RNG) $k-\varepsilon$ turbulence model, which is based on the transport equations of the turbulent kinetic energy (k) and dissipation rate (ε), was adopted (ANSYS, 2012; Zhou et al., 2018; Qi et al., 2019). The numerical solution was obtained with the finite volume method (FVM), and the semi-implicit method for pressure-linked equation (SIMPLE) algorithm was used as the pressure-correction principle (Patankar, 1980).

2.3.2. Lagrangian particles for visualizing flow trajectories

Sediment deposition and pollutant accumulation in the tunnel are of great concern. As there are facilities to retain bedload sediment before the inflow shaft at the surface, suspended sediment and dissolved pollutants in water are of great concern for management. Considering that the water velocity is high in the water filling process during storm events, suspended or dissolved components, such as suspended sediment and pollutants, mainly move along with the water flow. Hence, neutrally buoyant Lagrangian particles were introduced to visualize the flow trajectories of the initial inflow, suspended sediment, and dissolved pollutants. At the beginning of the numerical simulation, a total of 2 000 particles were released in the shafts containing inflow for each studied inflow conditions, and the moving trajectories were tracked during the water filling period. These neutrally buoyant particles did not influence multiphase flow calculations. It was similarly assumed that the evaluation of the trajectories of these neutrally buoyant particles provided insights into the distribution of sediment and dissolved particles in the tunnel following filling events.

2.3.3. Model setup

A 3-D compressible hydrodynamic and particle numerical model was developed with ANSYS Fluent. This model covered the Suzhou River DST comprising the main tunnel and two shafts (Fig. 3). The water flow was defined as compressible flow, and the reference density, the bulk modulus of elasticity, and the density exponent were set as 998.2 kg/m^3, 2.2 × 10^9 Pa, and 7.15, respectively. Air was considered compressible based on the ideal gas law (Hatcher et al., 2015; Zhou et al., 2018; Besharat et al., 2020). Heat conduction and convection in air, water, and pipe walls were calculated to represent the thermal processes during air pocket trapping.

In the numerical implementation of the DST, water inflows were input from the bottoms of the two shafts using the boundary conditions of the inflow discharge. Pressure boundary conditions were set at the tops of the two shafts, with the gage pressure set as zero. The walls of the main tunnel and shafts were defined as non-slip walls, with the roughness defined. Under the initial conditions, the tunnel and shafts were filled with air without water, and the velocity was assumed to be zero.

The numerical model was validated by comparing the air−water interface (Section 3.1) and tunnel pressure (Section 3.2) between the numerical simulation experiment and physical model test. Model validation procedures were inspired by the American Institute of Aeronautics and Astronautics (AIAA) Guide. With regards to the tunnel pressure, error statistics including the root mean square error (RMSE), RMSE-to-observation standard deviation ratio (RSR), and mean relative error (MRE) were used to assess the fitness (Roache, 1997, 2009; Moriasi et al., 2007).

2.3.4. Mesh independence analysis

Hexahedral and tetrahedral meshes were generated in the main tunnel and shafts, respectively. To assess the rationality of the mesh size, mesh independence analysis was conducted. Water pressures at station P1 (Fig. 3) under different average mesh size conditions were extracted (Fig. 4). The pressure head hydrographs showed that the pressure differences under different mesh size conditions were slight prior to the filling of the DST (from 0 to 1050 s), and the differences increased after DST filling. As observed in the physical model, a reduction in the average mesh size from 1.1 to 1.0 m or from 1.0 to 0.9 m did not significantly affect the overall pressure hydrograph and generated surges. The water−surface interface, surface wave, the compressibility of water and air, and energy equations were considered in the numerical model. In consideration of the calculation precision and efficiency, an average mesh size of 1.0 m was considered reasonable to simulate the hydrodynamic conditions in the DST, yielding a total mesh number of

Please cite this article as: He, W et al., Hydraulic characteristics and flow trajectories under two-sided asymmetric inflow conditions for a deep storage tunnel system, Water Science and Engineering, https://doi.org/10.1016/j.wse.2023.11.006

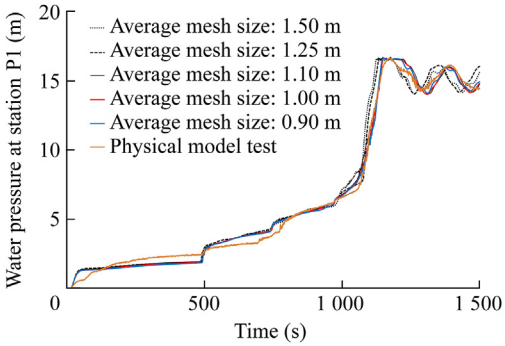

Fig. 4. Mesh independence analysis under scenario S1 with curves denoting water pressures at station P1 under different mesh size conditions.

195 959. The ANSYS mesh skewness parameter was considered adequate. Along the vertical direction, there were approximately 15 cells for the section, and the water surface could be identified with the VOF method.

2.4. Model scenarios

A baseline inflow scenario was set based on the hydrological estimates, which indicated that the design inflow discharges of the MP and YLX shafts should be fixed at 42.16 and 73.84 m^3/s, respectively. Indeed, runoff gradually increased under real rainstorm conditions. Under a low inflow, the water surface remained stable, the water pressure was low, and negative hydraulic influences were slight. Therefore, high peak inflows were mainly studied under different model scenarios. In addition to the baseline scenario, various inflow conditions, including one-sided (i.e., inflows entering from a single shaft) and two-sided inflow (i.e., inflows entering from two shafts), were considered in the 3-D simulations (Table 1). As previously stated, the operation scheme determined that the inflows must be shut down when the water pressure in the MP shaft reaches 15 m (a level of approximately 5 m above the tunnel crown) to avoid the occurrence of damaging surges. In the simulation of water filling, the inflow into the DST was stopped when the water level exceeded 5 m above the tunnel crown.

3. Results and discussion

3.1. Hydraulic characteristics and flow trajectories under two-sided asymmetric inflow scenario (S1)

3.1.1. Air–water interactions and particle trajectories

With the numerical calculation and physical model tests, the spatiotemporal fields of the velocity, air–water phase, pressure, turbulence, and particle movement were simulated. A description of the inflows and free surface created under the inflow scenario S1 was provided. Initially, the inflows entered the two-sided shafts, and they moved from the two shafts toward the middle of the tunnel apparatus. Two water surface mounds formed at the inflow fronts. The two inflow fronts collided and interacted with each other, causing a water level increase in the middle of the tunnel at 340 to 500 s (Fig. 5). Upon collision, the water flow direction was reversed, inducing reflected surface waves toward the two shafts. The water level then gradually increased near the shafts and decreased in the middle of the tunnel at approximately 580 s. Afterwards, the reflected surface waves arrived at the two shafts, and their directions were reversed again, causing a water level increase in the main tunnel (at 700 s). This process occurred repeatedly. The water level along the tunnel was uneven due to the surface waves, and a slope in the free surface was observed as the tunnel was filled with mixed free-surface and pressurized flows. Uneven water surface waves and a small fraction of entrapped air determined in the numerical simulations could be observed in the physical model tests at 1 060 and 1 120 s, respectively (Fig. 5).

A fraction of the air initially contained in the main tunnel, approximately 3.6% of the original volume, remained when the tunnel was pressurized, with more entrapped air in the upstream part of the tunnel than in the downstream part. Over time, with pressure oscillation and buoyancy, the simulation results and experimental observations indicated that the entrapped air was intermittently released from the tunnel through the shafts. The simulation results agreed with the observations in the experimental runs.

The neutrally buoyant tracer particles, which were added at the beginning of the numerical simulation, were transported with the water inflow and could be used to visualize the flow

Table 1
Numerical simulation model scenarios and physical model test.

Scenario	Description	Inflow discharge at MP shaft (m^3/s)		Inflow discharge at YLX shaft (m^3/s)	
		Prototype	Physical model	Prototype	Physical model
S1	Two-sided asymmetric inflow (baseline)	42.16	0.008 55	73.84	0.014 98
S2	Comparison of one- and two-sided inflows	42.16	0.008 55	0	0
S3		0	0	73.84	0.014 98
S4	Comparison of symmetric and asymmetric two-sided inflows	73.84	0.014 98	42.16	0.008 55
S5		58.00	0.011 77	58.00	0.011 77
S6	Comparison of different inflow discharges	42.16	0.008 55	42.16	0.008 55
S7		42.16	0.008 55	100.00	0.020 29

Please cite this article as: He, W et al., Hydraulic characteristics and flow trajectories under two-sided asymmetric inflow conditions for a deep storage tunnel system, Water Science and Engineering, https://doi.org/10.1016/j.wse.2023.11.006

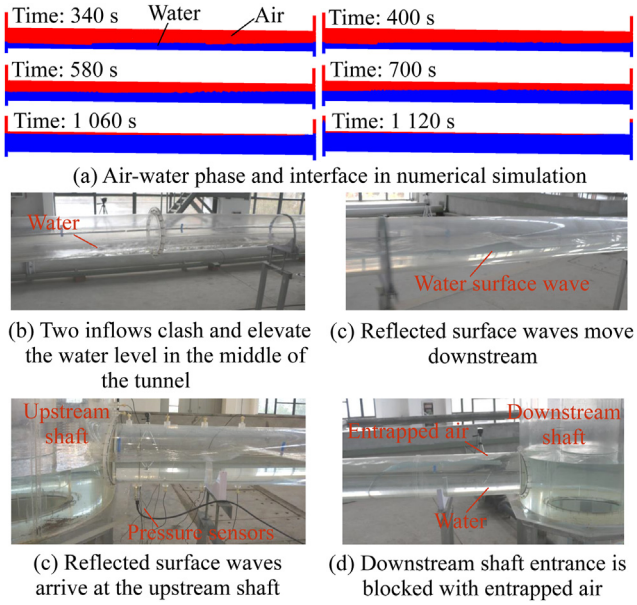

Fig. 5. Air–water interface in numerical simulation and physical model test (S1).

trajectories. As noted earlier, a similar assumption made in this study was that the evaluation of the trajectories of neutrally buoyant particles could provide insights into the distribution of sediment particles and dissolved pollutants in the tunnel following filling events.

As shown in Fig. 6(a), the design inflow conditions S1 yielded asymmetric flows that led to reversed flows, i.e., reversal of the velocity direction. First, the tracer particles moved from the two shafts toward the middle of the tunnel. The two inflow fronts collided and caused the generation of reflected surface waves, and the flow directions of some upstream particles were reversed because the upstream inflow

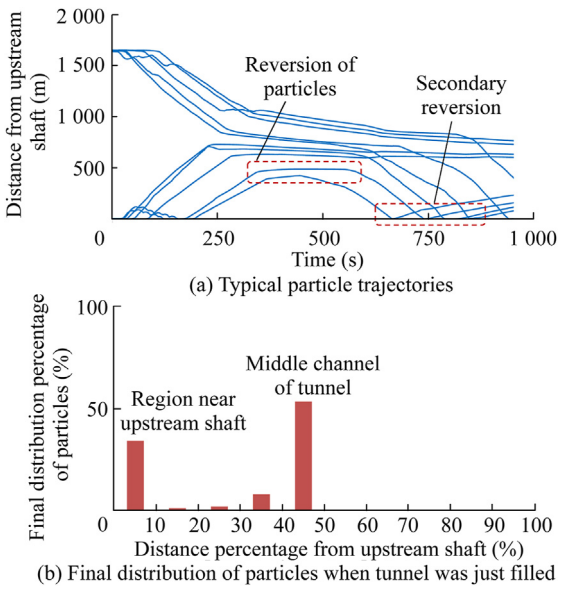

Fig. 6. Typical particle trajectories and final distribution of particles when tunnel was just filled under baseline scenario S1.

discharge (42.16 m^3/s) was lower than the downstream inflow discharge (73.84 m^3/s). Then, the flow directions of some particles were reversed again after arriving at the upstream shaft. As the downstream inflow was significantly higher than the upstream inflow, the moving directions of the particles originating from the downstream shaft hardly changed, and they remained near the middle of the tunnel. As the tunnel became pressurized, the particles were mainly distributed near the upstream shaft and the middle channel of the tunnel (0 and 50% from the upstream shaft, respectively) (Fig. 6(b)). Overall, the initial inflow water mainly flowed from the downstream areas with high inflow discharges to the upstream areas with low inflow discharges.

3.1.2. Pressure evolution and surging

Due to the movement and reflection of the water surface waves, the local water level successively increased along the tunnel, inducing a staggered pressure difference in the middle of the tunnel and near the shafts (Fig. 7). As shown in Fig. 7(a), the water pressures at the bottoms of the sections 0, 300, 600, and 900 m from the upstream MP shaft were extracted, and the measured values were scaled to the physical model using the Froude similarity principle. With regards to

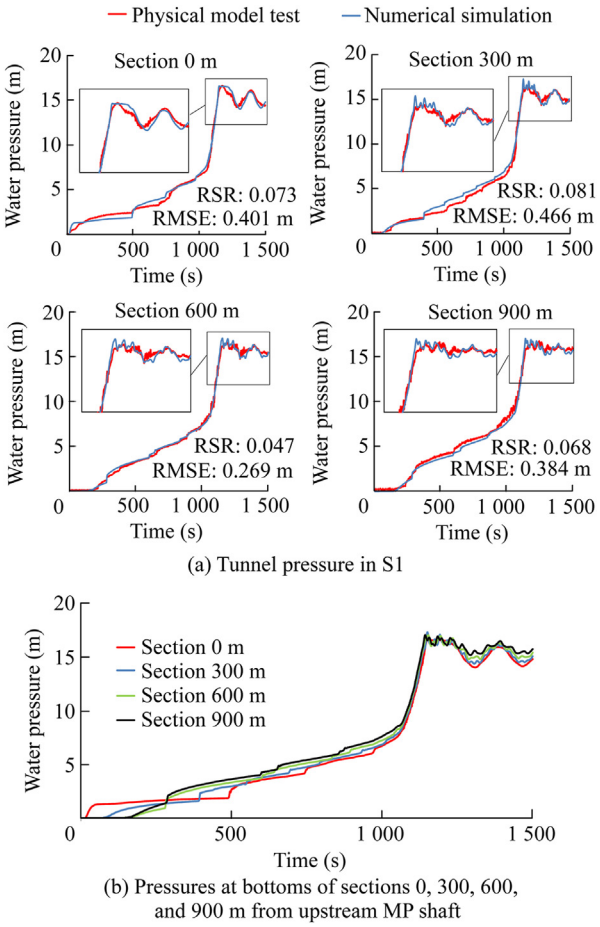

Fig. 7. Tunnel pressure in numerical simulation and experimental tests in S1 and pressures at bottoms of sections 0, 300, 600, and 900 m from upstream MP shaft.

Please cite this article as: He, W et al., Hydraulic characteristics and flow trajectories under two-sided asymmetric inflow conditions for a deep storage tunnel system, Water Science and Engineering, https://doi.org/10.1016/j.wse.2023.11.006

peak surging, the laboratory results and numerical predictions agreed with each other. RMSEs for the pressures at the bottoms of the sections 0, 300, 600, and 900 m were 0.401, 0.466, 0.269, and 0.384 m, respectively; and RSRs were 0.073, 0.081, 0.047, and 0.068, respectively, indicating rational fitness (Moriasi et al., 2007). The numerical simulation and physical model results showed a stepwise increasing trend at the stages when the tunnel was being filled, especially at 300, 600, and 900 m from the upstream MP shaft (Fig. 7(a)). This trend was more significant in the middle of the tunnel than near the shafts, and the pressure was successively higher or lower in the middle of the tunnel than near the shafts.

When the tunnel was filled, entrapped air was observed in the tunnel, and pressure oscillation occurred due to the entrapped air. The maximum fluctuation in the pressure was approximately 2.05 m from the average value. The oscillation amplitude was smaller in the middle of the tunnel than near the shafts due to the pressure counteraction effect of the surface wave from the two-sided shafts.

3.2. Hydraulic characteristics and flow trajectories under various inflow scenarios

3.2.1. Air–water interactions and particle trajectories

The design inflow conditions of the two-sided shafts (S1) were compared to the one-sided inflow scenarios, in which inflow entered either from the upstream shaft (S2) or from the downstream shaft (S3). As shown in Fig. 8, the inflows and particles moved from the inflow source toward the opposite shaft under these two scenarios. Final particle accumulation was observed in the shaft opposite to the inflow source (Fig. 9).

In the scenario with symmetric inflows entering from the two shafts, an uneven and more unstable free-surface profile over time was observed, relative to the design inflow conditions S1. Flow reversals, reflected surface waves, and secondary flow reversals were observed under the symmetric and asymmetric inflow scenarios (S1, S4, and S5). Fig. 8 shows that under the asymmetric inflow scenarios (S1 and S4), the initial inflow water mainly moved toward the shaft with lower inflows. Once the tunnel was pressurized, the particles accumulated toward the middle of the tunnel. Under the symmetric inflow scenario S5, Lagrangian particles first moved toward the middle of the tunnel and then moved toward the upstream shaft when the downstream shaft was filled (Fig. 8). Compared to scenario S4, scenario S5 showed slightly enhanced particle concentrations in the upstream portion of the tunnel when the filling process was completed (Fig. 9).

The results of scenarios S6 and S7 were compared. Scenario S6 used lower but symmetric inflows, and scenario S7 had higher inflows in the downstream shaft. Scenario S6 resembled scenario S1, but with less particle accumulation near the upstream shaft. Scenario S7, with higher inflows at the downstream end, led to higher particle concentrations in the upstream third of the tunnel.

3.2.2. Pressure variation and surging

When the tunnel was filled, stepwise increases in the pressure and staggered differences between the pressures in the middle of the tunnel and those near the shafts were consistently observed across the inflow scenarios. Such stepwise increases in the pressure were observed under the scenarios with a single inflow point (S2 and S3), but the absence of inflow front collision led to lower increases under scenarios S2 and S3 than under scenario S1 (Fig. 10(a)). Fig. 10(b) shows the pressure variation under the conditions with two inflow fronts (S1, S4, and S5). It shows that the pressure increased more significantly when two-sided inflow fronts collided in the tunnel.

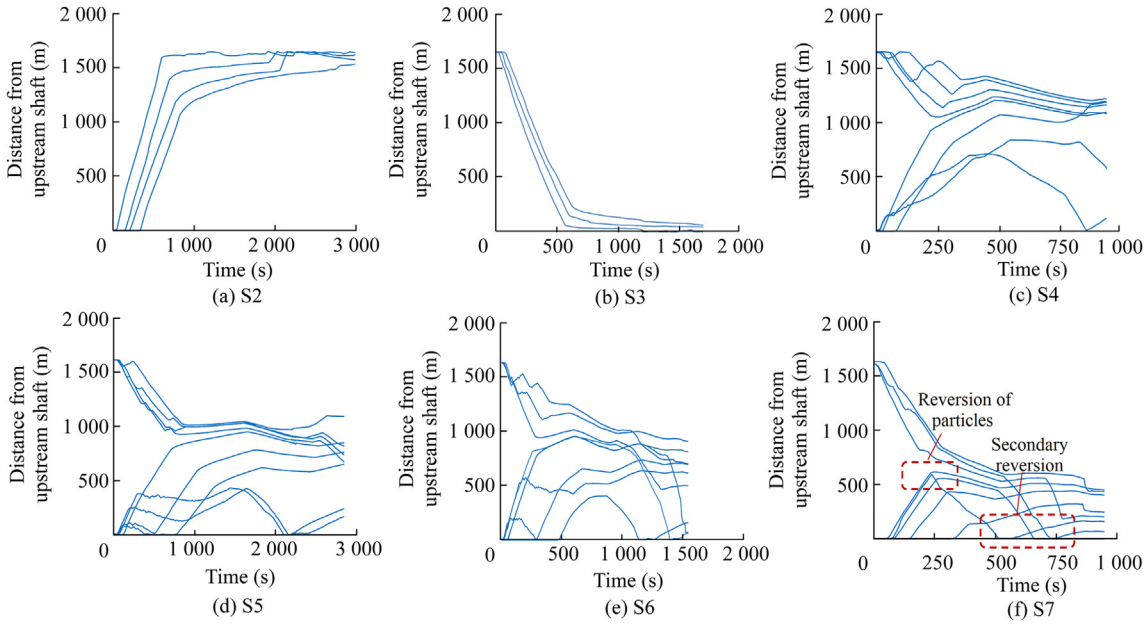

Fig. 8. Trajectories of typical particles under scenarios with one-sided inflows (S2 and S3), asymmetric inflows (S4 and S5), and different inflow discharges (S6 and S7).

Please cite this article as: He, W et al., Hydraulic characteristics and flow trajectories under two-sided asymmetric inflow conditions for a deep storage tunnel system, Water Science and Engineering, https://doi.org/10.1016/j.wse.2023.11.006

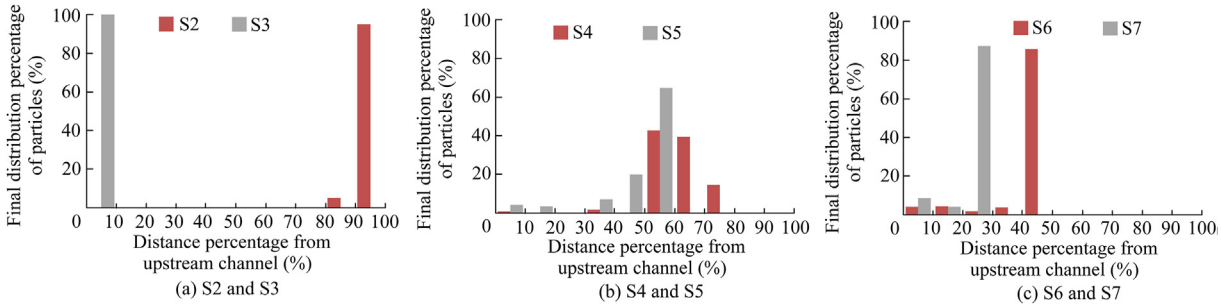

Fig. 9. Final distribution of particles along tunnel when tunnel became pressurized under scenarios S2 through S7.

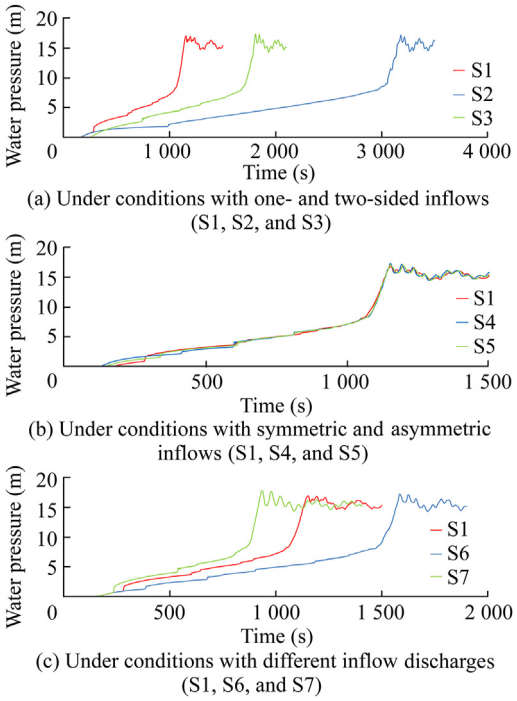

Fig. 10. Water pressure at bottom of section 600 m from upstream shaft under conditions with one- and two-sided inflows (S1, S2, and S3), symmetric and asymmetric inflows (S1, S4, and S5), and different inflow discharges (S1, S6, and S7).

As shown in Fig. 10, there was a rapid increase in the pressure once the tunnel became pressurized. In practice, when the water pressure in the MP shaft reaches 15 m (a level of approximately 5 m above the tunnel crown), the inflows are stopped by regulating a shaft gate to avoid the occurrence of damaging surges. The 3-D model showed that there was still a surge after the inflows were stopped. There was a general increase in peak surges with the admitted flow rates. The lowest peak surge calculated with the 3-D model at a distance (x) of 600 m from the upstream shaft was 17.07 m under scenario S1 (Table 2). The scenario with the greatest inflow, S7, yielded the largest pressure surge of 18.25 m at the same coordinate.

3.3. Prediction of sediment deposition and pollutant accumulation based on flow trajectory analysis

The initial volume of runoff during storm events always transports a mass of dissolved pollutants and suspended sediment, and the flow trajectories of the initial inflow determine sediment deposition and pollutant accumulation in the tunnel. Sediment deposition was predicted according to the final distribution of the particles (Fig. 9). Under the symmetric inflow scenarios (S5 and S6), the initial volume of the inflow water mainly moved toward the middle of the tunnel during most of the water-filling period (30% to 60% from the upstream shaft), where sediment deposition and pollutant accumulation occurred. Under all asymmetric inflow scenarios (S1, S2, S3, S4, and S7), particles accumulated near the shaft receiving less inflows. In the Suzhou River DST project, management should focus on sediment deposition and pollutant accumulation resulting from storm runoff in the upstream shaft and in the middle channel of the tunnel (0 and 40% from the upstream shaft; Fig. 9). The above locations are useful to predict the location where sediment accumulation is more likely to occur in the Suzhou DST and to implement treatment measures.

Table 2
Relationship between total inflow discharge and peak pressure head at bottoms of sections 0 and 600 m from upstream shaft.

Scenario	Combined flow (m^3/s)	Peak pressure head (m)	
		$x = 0$ m	$x = 600$ m
S1	116.00	16.61	17.07
S2	42.16	16.58	17.18
S3	73.84	16.62	17.38
S4	116.00	16.59	17.54
S5	116.00	16.60	17.30
S6	84.32	16.61	17.36
S7	142.16	16.62	18.25

3.4. Simulated entrapped air during tunnel filling

The total inflow discharge is considered the most important factor determining the percentage of the entrapped air, followed by the inflow distributions of the two shafts. Based on the simulation results in multiple scenarios, a positive relationship existed between the total inflow discharge and the percentage of the entrapped air. Therefore, a quadratic function could be used to fit this relationship under an initial water depth of 0 m (Fig. 11).

When the tunnel became pressurized, the inflows caused a slight reduction in the entrapped air under the one-sided inflow

Please cite this article as: He, W et al., Hydraulic characteristics and flow trajectories under two-sided asymmetric inflow conditions for a deep storage tunnel system, Water Science and Engineering, https://doi.org/10.1016/j.wse.2023.11.006

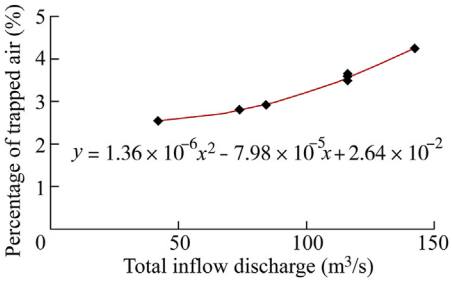

Fig. 11. Relationship between total inflow discharge and percentage of entrapped air in tunnel under initial water depth of 0 m.

conditions (scenarios S2 and S3), compared to the scenarios with two-sided inflows from the shafts. The entrapped air under the scenarios with one-sided inflows (S2 and S3) led to air pocket volumes of 2.55% and 2.80%, respectively. The scenarios with two symmetric inflows yielded larger air pocket volumes. Under inflow scenarios S1, S4, and S5, the percentages of the entrapped air along the tunnel were 3.57%, 3.50%, and 3.59%, respectively. Analysis of the 3-D model results indicated that when the tunnel became pressurized, the asymmetric inflow scenarios exhibited reduced reflected surface waves and decreased the entrapped air volumes, relative to the symmetric inflow scenarios. The scenario with the greatest inflow rate (S7) exhibited the highest fraction of the entrapped air (4.24%). The 3-D model results indicated an increase in the entrapped air pocket volume with the inflow discharge.

3.5. Prospects of this study

Future research directions are recommended as follows. First, this study mainly focused on only one section of the DST with two inflow shafts. Two or more tunnel sections with multiple shafts will be studied. With regards to two or more tunnel sections with three or more inflow shafts, the interactions originating from further downstream sections can also propagate to upstream sections, causing significant pressure and water surface differences from two-sided inflow scenarios. Second, along the vertical direction, there were approximately 15 cells for the section. Although the water surface could be identified with the VOF method, the cells should be further refined to better capture the water−air surface, air volume change, etc. Finally, as there are facilities to retain bedload sediment before the inflow shaft at the surface of the Suzhou River DST, the deposition of suspended sediment was mainly predicted with neutrally buoyant particles in this study. As there exists an inherent difference between sediment and neutrally buoyant particles, a real sediment model to simulate the start and deposition of sediment should be embedded in the numerical model, and the bedload type should be further considered.

4. Conclusions

Hydraulic characteristics and flow trajectories significantly influence the structural safety, sediment deposition, and pollutant accumulation in a deep tunnel. In this study, a 3-D compressible hydrodynamic and particle numerical model was developed to capture air−water interactions and particle trajectories and simulate peak surges. According to the 3-D numerical simulation and physical model test results, the flow pattern and trajectory, air−water phase, and water pressure in the Suzhou River DST were analyzed under various inflow conditions. The main conclusions are as follows.

(1) Under the scenarios with two-sided inflows, reversed flows and surface waves occurred, in contrast to the scenarios with one-sided inflow. Stepwise increases in the pressure were consistently observed, and there were staggered differences between the pressures in the middle of the tunnel and those near the shafts, which was dependent on specific inflow scenarios.

(2) Under the asymmetric two-sided inflow scenarios, the trajectories of water particles were oriented toward the shaft with a lower inflow. Similarly, with an assumption that neutrally buoyant particles represented suspended sediment and dissolved pollutants, the Suzhou River DST likely exhibited more significant sediment and pollutant accumulation in the middle channel of the tunnel (0 and 50% from the upstream shaft). Under the symmetric inflow conditions, accumulation could occur closer to the midpoint of the tunnel.

(3) Regarding the modeled entrapment of air, the scenarios with the one-sided inflow conditions led to smaller entrapped air volumes than the scenarios with two-sided inflows. The increasing inflows led to larger entrapped air volumes, with the greatest fraction observed under scenario S7, exceeding 4.2%.

DSTs play important roles in regulating storm runoff and reducing runoff pollution in highly urbanized cities, which should be sufficiently considered in future urban planning. With the increasing focus on urban water safety and the environment, research in this field should consider more geometric types of DSTs, including various structural types of tunnels and shafts, as well as more diverse inflow scenarios involving various intense rain events linked with climate change scenarios.

Declaration of competing interest

The authors declare no conflicts of interest.

References

ANSYS, 2012. ANSYS FLUENT Theory Guide. ANSYS, Inc., Canonsburg.

Besharat, M., Coronado-Hernández, O.E., Fuertes-Miquel, V.S., Viseu, M.T., Ramos, H.M., 2020. Computational fluid dynamics for sub-atmospheric pressure analysis in pipe drainage. J. Hydraul. Res. 58(4), 553−565. https://doi.org/10.1080/00221686.2019.1625819.

Catano-Lopera, Y.A., Tokyay, T.E., Ezequiel Martin, J., Schmidt, A.R., Lanyon, R., Fitzpatrick, K., Scalise, C.F., Garcia, M.H., 2014. Modeling of a transient event in the tunnel and reservoir plan system in Chicago, Illinois. J. Hydraul. Eng. 140(9), 05014005. https://doi.org/10.1061/(ASCE)HY.1943-7900.0000888.

Chanson, H., Gualtieri, C., 2008. Similitude and scale effects of air entrainment in hydraulic jumps. J. Hydraul. Res. 46(1), 35−44. https://doi.org/10.1080/00221686.2008.9521841.

Please cite this article as: He, W et al., Hydraulic characteristics and flow trajectories under two-sided asymmetric inflow conditions for a deep storage tunnel system, Water Science and Engineering, https://doi.org/10.1016/j.wse.2023.11.006

Cheng, Y., Li, J., Yang, J., 2010. Free surface-pressurized flow in ceiling-sloping tailrace tunnel of hydropower plant: Simulation by VOF model. J. Hydraul. Res. 45(1), 88−99. https://doi.org/10.1080/00221686.2007.9521747.

Duan, H., 2015. Uncertainty analysis of transient flow modeling and transient-based leak detection in elastic water pipeline systems. Water Resour. Manag. 29(14), 5413−5427. https://doi.org/10.1007/s11269-015-1126-4.

Eldayih, Y., Cetin, M., Vasconcelos, J.G., 2020. Air-pocket entrapment caused by shear flow instabilities in rapid-filling pipes. J. Hydraul. Eng. 146, 040200164. https://doi.org/10.1061/(ASCE)HY.1943-7900.0001711.

Epstein, M., 2008. A simple approach to the prediction of waterhammer transients in a pipe line with entrapped air. Nucl. Eng. Des. 238(9), 2182−2188. https://doi.org/10.1016/j.nucengdes.2008.02.023.

Gualtieri, C., Chanson, H., 2021. Physical and numerical modelling of air−water flows: An introductory overview. Environ. Model. Software 143, 105109. https://doi.org/10.1016/j.envsoft.2021.105109.

Guo, X., Zhou, Y., 2006. Precise integration method for numerical simulation of transient mixed free-surface-pressure flow. J. Hydrodyn. 21(4), 533−537 (in Chinese).

Hatcher, T.M., Malekpour, A., Vasconcelos, J., Karney, B., 2015. Comparing unsteady modeling approaches of surges caused by sudden air pocket compression. Journal of Water Managment Modelling 23, C392. https://doi.org/10.14796/JWMM.C392.

Hatcher, T.M., Vasconcelos, J.G., 2017. Peak pressure surges and pressure damping following sudden air pocket compression. J. Hydraul. Eng. 143, 040160944. https://doi.org/10.1061/(ASCE)HY.1943-7900.0001251.

He, W., Lian, J., Ma, C., Wu, M., Liu, F., 2017. Analysis of the thrust force on the temperature-control curtain in a large stratified reservoir. J. Hydraul. Eng. 143(12), 4017049. https://doi.org/10.1061/(ASCE)HY.1943-7900.0001378.

He, W., Lian, J., Liu, F., Ma, C., Pan, S., 2018. Experimental and numerical study on the thrust of a water-retaining curtain. J. Hydroinf. 20(2), 316−331. https://doi.org/10.2166/hydro.2017.095.

Higuchi, K., Maeda, M., Shintani, Y., 1994. Sewer system for improving flood control in Tokyo: A step towards a return period of 70 years. Water Sci. Technol. 29(1−2), 303−310. https://doi.org/10.2166/wst.1994.0677.

Hirt, C.W., Nichols, B.D., 1981. Volume of fluid (VOF) method for the dynamics of free boundaries. J. Comput. Phys. 39(1), 201−225. https://doi.org/10.1016/0021-9991(81)90145-5.

Leon, A., Oberg, N., Schmidt, A.R., Garcia, M.H., 2011. Illinois transient model: Simulating the flow dynamics in combined storm sewer systems. Journal of Water Management Modelling 19, R241. https://doi.org/10.14796/JWMM.R241-02. -02.

Li, L., Zhu, D., Huang, B., 2018. Analysis of pressure transient following rapid filling of a vented horizontal pipe. Water 10(11), 1698. https://doi.org/10.3390/w10111698.

Lingireddy, S., Wood, D.J., Zloczower, N., 2004. Pressure surges in pipeline systems resulting from air releases. J. Am. Water Works Assoc. 96(7), 88−94. https://doi.org/10.1002/j.1551-8833.2004.tb10652.x.

Malekpour, A., Karney, B., 2019. Complex interactions of water, air and its controlled removal during pipeline filling operations. Fluid Mech. Res. Int. J. 3(1), 4−15. https://doi.org/10.15406/fmrij.2019.03.00046.

Moriasi, D.N., Arnold, J.G., Van Liew, M.W., Bingner, R.L., Harmel, R.D., Veith, T.L., 2007. Model evaluation guidelines for systematic quantification of accuracy in watershed simulations. Trans. ASABE (Am. Soc. Agric. Biol. Eng.) 50(3), 885−900. https://doi.org/10.13031/2013.23153.

Pachaly, R.L., Vasconcelos, J.G., Allasia, D.G., Tassi, R., Bocchi, J.P.P., 2020. Comparing SWMM 5.1 calculation alternatives to represent unsteady stormwater sewer flows. J. Hydraul. Eng. 146, 040200467. https://doi.org/10.1061/(ASCE)HY.1943-7900.0001762.

Pachaly, R.L., Vasconcelos, J.G., Allasia, D.G., 2021. Surge predictions in a large stormwater tunnel system using SWMM. Urban Water J. 18(8), 577−584. https://doi.org/10.1080/1573062X.2021.1916828.

Patankar, S.V., 1980. Numerical Heat Transfer and Fluid Flow. Hemisphere, Washington, DC.

Pfister, M., Chanson, H., 2014. Two-phase air−water flows: Scale effects in physical modeling. J. Hydrodyn. 26(2), 291−298. https://doi.org/10.1016/S1001-6058(14)60032-9.

Qi, Y., Wang, Y., Zhang, J., 2019. Three-dimensional turbulence numerical simulation of flow in a stepped dropshaft. Water 11(1), 30. https://doi.org/10.3390/w11010030.

Roache, P.J., 1997. Quantification of uncertainty in computational fluid dynamics. Annu. Rev. Fluid Mech. 29, 123−160. https://doi.org/10.1146/annurev.fluid.29.1.123.

Roache, P.J., 2009. Perspective: Validation—what does it mean? J. Fluid Eng. 131(3), 034503. https://doi.org/10.1115/1.3077134.

Schulz, H.E., Vasconcelos, J.G., Patrick, A.C., 2020. Air entrainment in pipe-filling bores and pressurization interfaces. J. Hydraul. Eng. 146, 040190532. https://doi.org/10.1061/(ASCE)HY.1943-7900.0001672.

Song, C.C.S., Cardie, J.A., Leung, K.S., 1983. Transient mixed-flow models for storm sewers. J. Hydraul. Eng. 109(11), 1487−1504.

Vasconcelos, J.G., Wright, S.J., 2003. Surge associated with air expulsion in near-horizontal pipelines. In: Proceedings of FEDSM'03, the 4th ASME_JSME Joint Fluids Engineering Conference. ASME, Honolulu.

Vasconcelos, J.G., Wright, S.J., 2006. Mechanisms for air pocket entrapment in stormwater storage tunnels. In: Proceedings of the World Environmental and Water Resources Congress 2006. ASCE, Omaha.

Vasconcelos, J.G., Wright, S.J., Roe, P.L., 2009. Numerical oscillations in pipe-filling bore predictions by shock-capturing models. J. Hydraul. Eng. 135(4), 296−305.

Vasconcelos, J.G., Wright, S.J., 2017. Anticipating transient problems during the rapid filling of deep stormwater storage tunnel systems. J. Hydraul. Eng. 143, 060160253. https://doi.org/10.1061/(ASCE)HY.1943-7900.0001250.

Wang, J., Vasconcelos, J.G., 2018. Geyser episodes created by the release of a sequence of discrete air pockets in vertical shafts. In: Proceedings of the World Environmental and Water Resources Congress 2018. ASCE, Beijing. https://doi.org/10.1061/9780784481424.001.

Wang, J., Vasconcelos, J.G., 2020. Investigation of manhole cover displacement during rapid filling of stormwater systems. J. Hydraul. Eng. 146, 040200224. https://doi.org/10.1061/(ASCE)HY.1943-7900.0001726.

Wang, L., Zhang, J., Liao, Q., Tan, Q., 2016. Research on deep drainage tunnel project planning of Suzhou River. China Water & Wastewater 32(15), 139−142 (in Chinese).

Wright, S.J., Lewis, J.W., Vasconcelos, J.G., 2011. Geysering in rapidly filling storm-water tunnels. J. Hydraul. Eng. 137(1), 112−115. https://doi.org/10.1061/(ASCE)HY.1943-7900.0000245.

Wu, H., Huang, G., Meng, Q., Zhang, M., Li, L., 2016. Deep tunnel for regulating combined sewer overflow pollution and flood disaster: A case study in Guangzhou City, China. Water 8(8), 329. https://doi.org/10.3390/w8080329.

Zhao, W., Zhang, J., He, W., Zhang, T., Wang, S., Shi, L., 2022. Hydrodynamic characteristics of lateral withdrawal with effects of the slope ratio. AQUA - Water Infrastructure, Ecosystems and Society 71(1), 72−85. https://doi.org/10.2166/aqua.2021.222.

Zhou, L., Wang, H., Karney, B., Liu, D., Wang, P., Guo, S., 2018. Dynamic behavior of entrapped air pocket in a water filling pipeline. J. Hydraul. Eng. 144(8), 4018045. https://doi.org/10.1061/(ASCE)HY.1943-7900.0001491.

Please cite this article as: He, W et al., Hydraulic characteristics and flow trajectories under two-sided asymmetric inflow conditions for a deep storage tunnel system, Water Science and Engineering, https://doi.org/10.1016/j.wse.2023.11.006